Stanford Exploration Project, Report 123, October 31, 2005, pages 129–154

Mapping of water-bottom and diffracted 2D multiple reflections to image space

Gabriel Alvarez[1]

ABSTRACT

Wave-equation migration with the velocity of the primaries maps non-diffracted water-bottom multiples to an hyperbola in subsurface-offset-domain-common-image-gathers. Furthermore, for positive surface offsets, the multiples are mapped to non-positive subsurface offsets if sediment velocity is faster than water. The larger the offset in the data space, the larger the subsurface offset and the shallower the image point. When migrated with the velocity of the water, the multiples are mapped to zero subsurface offset just as primaries migrated with the exact velocity. Diffracted multiples, on the other hand, map to positive or negative subsurface offsets depending on the relative position of the diffractor with respect to the common-midpoint. I present the equations of the image point coordinates in terms of the data space coordinates for diffracted and non-diffracted multiples from flat or dipping water-bottom in both subsurface-offset-domain common-image-gathers and angle-domain common-image-gathers. I illustrate the results with simple synthetic models.

INTRODUCTION

Attenuation of multiples in the image space is attractive because prestack wave-equation migration accurately handles the complex wave propagation of primaries. In subsurface-offset-domain common-image-gathers (SODCIG) the primaries are imaged at zero subsurface offset at the depth of the reflector if migrated with the correct velocity. Correspondingly, in angle-domain common-image-gathers (ADCIG) the primaries are imaged with flat moveout. Attenuation of multiples in image space depends on the difference in residual moveout between the primaries and the multiples, either in SODCIGs or ADCIGs (Sava and Guitton, 2003; Hargreaves et al., 2003; Alvarez et al., 2004). Understanding how wave-equation migration maps the multiples into SODCIGs and ADCIGs is therefore of paramount importance in order to design a proper strategy to attenuate the multiples in the image space.

Non-diffracted water-bottom multiples from a flat or dipping water-bottom are imaged as primaries. Thus, if the migration velocity is that of the water, they are mapped to zero

[1]**email:** gabriel@sep.stanford.edu

subsurface-offset in SODCIGs. Consequently, in ADCIGs, these multiples exhibit flat moveout just as primaries do (Alvarez, 2005). In the usual case of migration with velocities faster than water velocity, these multiples are mapped to subsurface offsets with the opposite sign with respect to the sign of the surface offsets. I will analytically show the moveout curve of these multiples in SODCIGs and ADCIGs.

Water-bottom diffracted multiples, on the other hand, even if from a flat water-bottom, do not migrate as primary reflections (Alvarez, 2005). That is, they do not focus to zero subsurface offset even if migrated with the water velocity. Obviously this happens because at the diffractor the reflection is not specular. I will show that these multiples migrate to both positive and negative subsurface offsets in SODCIGs depending on the relative position of the diffractor with respect to the receiver (for receiver-side diffracted multiples).

The next section presents a general formulation for computing the kinematics of diffracted and non-diffracted water-bottom multiples for both SODCIGs and ADCIGs. The following section then looks in detail at the special case of flat water-bottom where the equations simplify and some insight can be gained as to the analytical representation of the residual moveout of the multiples in both SODCIGs and ADCIGs. The next section presents a similar result for multiples from a dipping water-bottom. Although the equations are more involved and difficult to encapsulate in one single expression than those for the flat water-bottom, I show that we can still compute the image space coordinates of both the diffracted and non-diffracted multiples in terms of their data space coordinates. The last section discusses some of the implications of the results and the possibility that they can be used to attenuate the multiples in the image space. Detailed derivation of all the equations is included in the appendices.

KINEMATICS OF WATER-BOTTOM MULTIPLES IN IMAGE SPACE

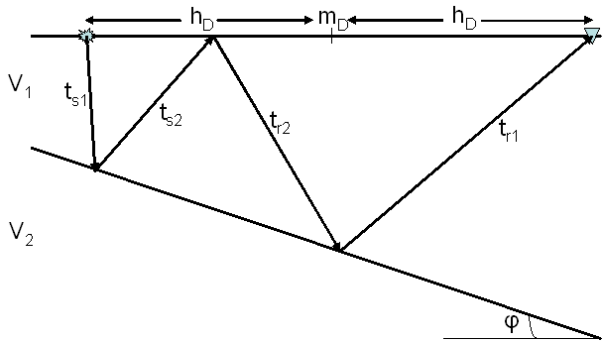

Figure 1: Water-bottom multiple. The subscript s refers to the source and the subscript r to the receiver. gabriel1-mul_sktch1 [NR]

The propagation path of a water-bottom multiple, as shown in Figure 1, consists of four segments, such that the total travel-time for the multiple is given by

$$t_m = t_{s_1} + t_{s_2} + t_{r_2} + t_{r_1}, \tag{1}$$

where the subscript s refers to the source-side rays and the subscript r refers to the receiver-side rays. The data space coordinates are (m_D, h_D, t_m) where m_D is the horizontal position of the CMP gather and h_D is the half-offset between source and receiver. Wave-equation

migration maps the CMP gathers to SODCIGs with coordinates (m_ξ, h_ξ, z_ξ) where m_ξ is the horizontal position of the image gather, and h_ξ and z_ξ are the half subsurface-offset and the depth of the image, respectively. As illustrated in the sketch of Figure 2, at any given depth

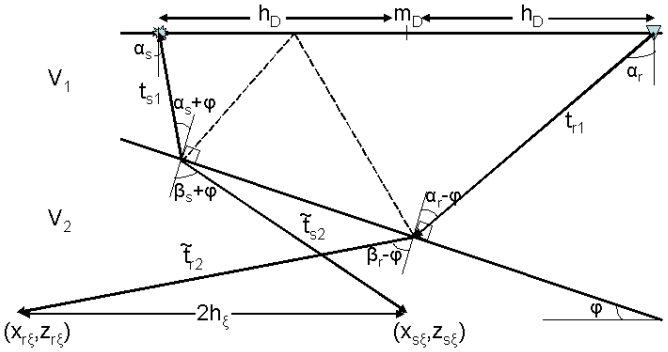

Figure 2: Imaging of water-bottom multiple in SODCIG. The subscript ξ refers to the image point. gabriel1-mul_sktch2 [NR]

the image space coordinates of the migrated multiple are given by:

$$
\begin{aligned}
x_{s_\xi} &= m_D - h_D + V_1(t_{s_1}\sin\alpha_s + \rho\tilde{t}_{s_2}\sin\beta_s), \\
x_{r_\xi} &= m_D + h_D - V_1(t_{r_1}\sin\alpha_r + \rho\tilde{t}_{r_2}\sin\beta_r), \\
h_\xi &= \frac{x_{r_\xi} - x_{s_\xi}}{2} = h_D - \frac{V_1}{2}\left[t_{s_1}\sin\alpha_s + t_{r_1}\sin\alpha_r + \rho(\tilde{t}_{s_2}\sin\beta_s + \tilde{t}_{r_2}\sin\beta_r)\right], \qquad (2)\\
z_\xi &= V_1(t_{s_1}\cos\alpha_s + \rho\tilde{t}_{s_2}\cos\beta_s) = V_1(t_{r_1}\cos\alpha_r + \rho\tilde{t}_{r_2}\cos\beta_r), \qquad (3)\\
m_\xi &= \frac{x_{r_\xi} + x_{s_\xi}}{2} = m_D + \frac{V_1}{2}\left(t_{s_1}\sin\alpha_s - t_{r_1}\sin\alpha_r + \rho(\tilde{t}_{s_2}\sin\beta_s - \tilde{t}_{r_2}\sin\beta_r)\right), \qquad (4)
\end{aligned}
$$

where V_1 is the water velocity, $\rho = V_2/V_1$ with V_2 the sediment velocity, and α_s, α_r are the acute takeoff angles of the source and receiver rays with respect to the vertical. The traveltime of the refracted ray segments $\tilde{t}_{s_2}$ and $\tilde{t}_{r_2}$ can be computed from two conditions: (1) at the image point the depth of both rays has to be the same (since we are computing horizontal subsurface offset gathers) and (2) $t_{s_2} + t_{r_2} = \tilde{t}_{s_2} + \tilde{t}_{r_2}$ which follows immediately from equation 1 since at the image point the extrapolated time equals the traveltime of the multiple. As shown in Appendix A, the traveltimes of the refracted rays are given by

$$
\begin{aligned}
\tilde{t}_{s_2} &= \frac{t_{r_1}\cos\alpha_r - t_{s_1}\cos\alpha_s + \rho(t_{s_2} + t_{r_2})\cos\beta_r}{\rho(\cos\beta_s + \cos\beta_r)}, \qquad (5)\\
\tilde{t}_{r_2} &= \frac{t_{s_1}\cos\alpha_s - t_{r_1}\cos\alpha_r + \rho(t_{s_2} + t_{r_2})\cos\beta_s}{\rho(\cos\beta_s + \cos\beta_r)}. \qquad (6)
\end{aligned}
$$

The refracted angles are related to the takeoff angles by Snell's law: $\sin(\beta_s+\varphi) = \rho\sin(\alpha_s+\varphi)$ and $\sin(\beta_r-\varphi) = \rho\sin(\alpha_r-\varphi)$, from which we get

$$
\begin{aligned}
\sin\beta_s &= \rho\sin(\alpha_s+\varphi)\cos\varphi - \sqrt{1-\rho^2\sin^2(\alpha_s+\varphi)}\sin\varphi, \qquad (7)\\
\sin\beta_r &= \rho\sin(\alpha_r-\varphi)\cos\varphi + \sqrt{1-\rho^2\sin^2(\alpha_r-\varphi)}\sin\varphi, \qquad (8)\\
\cos\beta_s &= \sqrt{1-\rho^2\sin^2(\alpha_s+\varphi)}\cos\varphi + \rho\sin(\alpha_s+\varphi)\sin\varphi, \qquad (9)\\
\cos\beta_r &= \sqrt{1-\rho^2\sin^2(\alpha_r-\varphi)}\cos\varphi - \rho\sin(\alpha_r-\varphi)\sin\varphi. \qquad (10)
\end{aligned}
$$

Equations 2–10 are valid for any water-bottom multiple, whether from a flat or dipping water-bottom. They even describe the migration of source- or receiver-side diffraction multiples, since no assumption has been made relating α_r and α_s or the individual traveltime segments. In ADCIGs, the mapping of the multiples can be directly related to the previous equations by

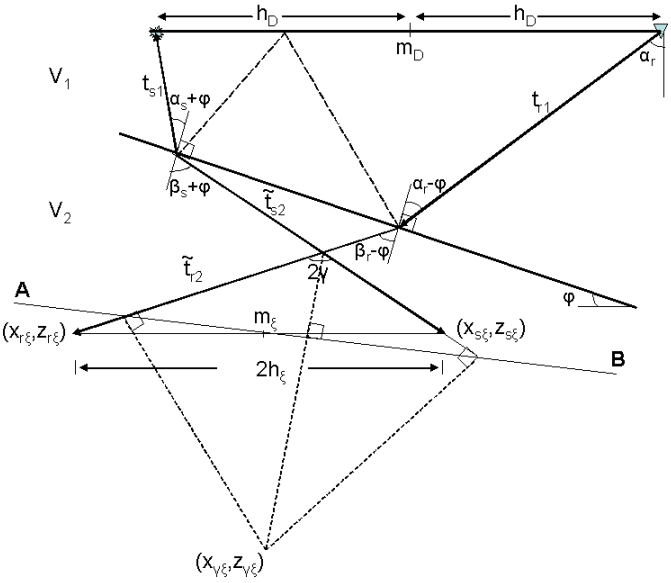

Figure 3: Imaging of water-bottom multiple in ADCIG. The subscript ξ refers to the image point. The line AB represents the apparent reflector at the image point. gabriel1-mul_sktch3 [NR]

the geometry shown in Figure 3. The half-aperture angle is given by

$$\gamma = \frac{\beta_r + \beta_s}{2}, \tag{11}$$

which is the same equation used for converted waves (Rosales and Biondi, 2005). The depth of the image point (z_{ξ_γ}) is given by (Appendix B)

$$z_{\xi_\gamma} = z_\xi - h_\xi \tan\gamma. \tag{12}$$

Equations 2–12 formally describe the image coordinates in terms of the data coordinates. They are, however, of little practical use unless we can relate the individual traveltime segments (t_{s_1}, t_{s_2}, $\tilde{t}_{s_2}$, t_{r_2}, $\tilde{t}_{r_2}$, t_{r_1}), and the angles α_s and α_r (which in turn determine β_s and β_r) to the known data space parameters (m_D, h_D, t_m, V_1, φ and ρ). This may not be easy or even possible analytically for all situations, but it is for some simple but important models that I will now examine.

FLAT WATER-BOTTOM

Non-diffracted multiple

The traveltime of the water-bottom multiple is given by (Alvarez, 2005)

$$t_m = \frac{4}{V_1}\sqrt{\left(\frac{h_D}{2}\right)^2 + Z_{wb}^2} = \sqrt{t_m^2(0) + \left(\frac{2h_D}{V_1}\right)^2}, \tag{13}$$

which is simply the traveltime of a primary at twice the depth of the water-bottom $Z_{wb} = \frac{V_1 t_m(0)}{4}$. From Figure 4 it is clear that due to the symmetry of the problem, $t_{s_1} = t_{s_2} = t_{r_1} =$

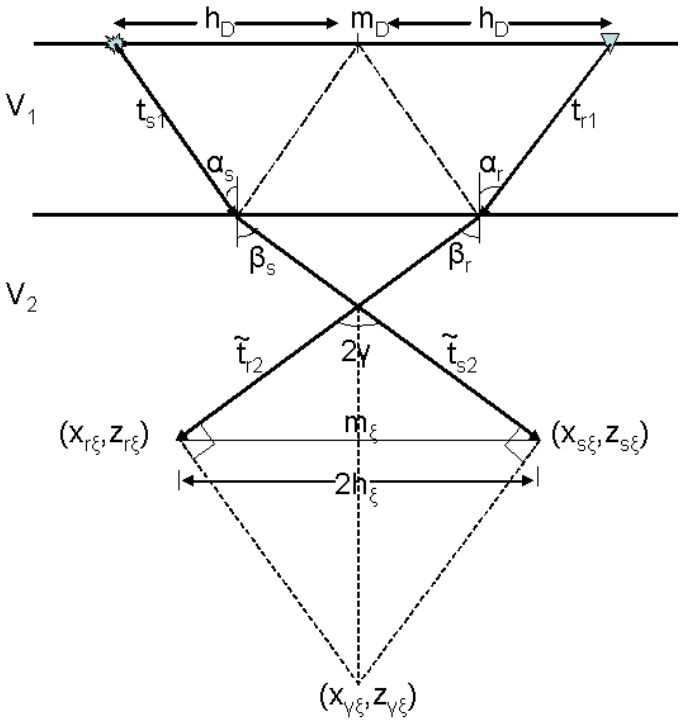

Figure 4: Imaging of water-bottom multiple for a flat water-bottom. Notice that $m_D = m_\xi$ and that the apparent reflector at the image point is flat. gabriel1-mul_sktch4 [NR]

$t_{r_2} = t_m/4$ and $\alpha_s = \alpha_r$, which in turn means $\beta_s = \beta_r$. Furthermore, from Equations 5 and 6 it immediately follows that $\tilde{t}_{s_2} = t_{s_2}$ and $\tilde{t}_{r_2} = t_{r_2}$ which says that the traveltimes of the refracted rays are equal to the corresponding traveltimes of the multiple. Equation 2 thus simplifies to

$$h_\xi = \frac{h_D}{2}(1-\rho^2), \tag{14}$$

which indicates that the subsurface offset at the image point of a trace with half surface offset h_D depends only on the velocity contrast between the water and the sediments. In particular, if the trace is migrated with the water velocity, *i.e.* $\rho = 1$, then $h_\xi = 0$ which proves the claim that the trace is imaged exactly as a primary since it is mapped to zero subsurface offset irrespective of its surface offset. It should also be noted that, since usually sediment velocity is faster than water velocity, then $\rho^2 > 1$ and therefore the multiples are mapped to subsurface offsets with the opposite sign with respect to the sign of the surface offset h_D when migrated with sediment velocity.

From Equation 3, the depth of the image point can be easily computed as

$$z_\xi = Z_{wb} + \frac{\rho}{2}\sqrt{h_D^2(1-\rho^2) + 4Z_{wb}^2}, \tag{15}$$

which for migration with the water velocity reduces to $z_\xi = 2Z_{wb}$, which shows that the multiple is migrated as a primary at twice the water depth. Finally, from Equation 4, the horizontal position of the image point reduces to

$$m_\xi = m_D. \tag{16}$$

This result shows that the multiple is mapped in the image space to the same horizontal position as the corresponding CMP even if migrated with sediment velocity. This result is obviously a direct consequence of the symmetry of the raypaths of the multiple reflection in this case.

Equations 14–16 give the image space coordinates in terms of the data space coordinates. An important issue is the functional relationship between the subsurface offset and the image depth, since it determines the moveout of the multiples in the subsurface-offset-domain common-image-gathers (SODCIGs). Replacing $h_D = 2h_\xi/(1-\rho^2)$ and $Z_{wb} = z_\xi(0)/(1+\rho)$ in Equation 15 we get

$$z_\xi = \frac{z_\xi(0)}{1+\rho} + \rho\sqrt{\left(\frac{z_\xi(0)}{1+\rho}\right)^2 + \frac{h_\xi^2}{1-\rho^2}} \qquad (\rho \neq 1) \tag{17}$$

which shows that the moveout is an hyperbola (actually half of an hyperbola since we already established that $h_\xi \leq 0$ if $h_D \geq 0$). Figure 5 shows an SODCIG for a non-diffracted water-

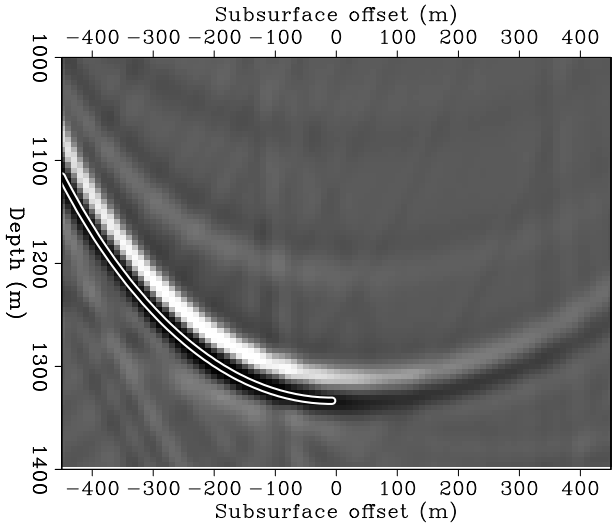

Figure 5: Subsurface offset domain common image gather of a water-bottom multiple from a flat water-bottom. Water velocity is 1500 m/s, water depth 500 m, sediment velocity 2500 m/s and surface offsets from 0 to 2000 m. Overlaid is the residual moveout curve computed with Equation 17. gabriel1-odcig1 [CR]

bottom multiple from a flat water-bottom 500 m deep. The data was migrated with a two-layer velocity model: the water layer of 1500 m/s and a sediment layer of velocity 2500 m/s. Larger subsurface offsets (which according to Equation 14 correspond to larger surface offsets) map to shallower depths (for the normal situation of $\rho > 1$), as we should expect since the rays are refracted to increasingly larger angles until the critical reflection angle is reached. Also notice that the hyperbola is shifted down by a factor $(1+\rho)$ with respect to the image point when migrated with water velocity.

In angle-domain common-image-gathers (ADCIGs), the half-aperture angle reduces to $\gamma = \beta_s = \beta_r$, which in terms of the data space coordinates is given by

$$\gamma = \sin^{-1}\left[\frac{2\rho h_D}{V_1 t_m}\right]. \tag{18}$$

The depth of the image can be easily computed from Equation 12. In particular, if the data are migrated with the velocity of the water, $\rho = 1$, and therefore $z_{\xi\gamma} = 2Z_{wb}$ which means a

horizontal line in the (z_{ξ_γ},γ) plane. Equivalently, we can say that the residual moveout in the (z_{ξ_γ},γ) plane is zero, once again corroborating that the water-bottom multiple is migrated as a primary if $\rho=1$. Equation 12 can be expressed in terms of the data space coordinates using Equations 14 and 15 and noting that

$$\tan\gamma=\tan\beta_s=\frac{\rho\sin\alpha_s}{\sqrt{1-\rho^2\sin^2\alpha_s}}=\frac{2\rho h_D}{\sqrt{V_1^2t_m^2-4\rho^2h_D^2}}=\frac{\rho h_D}{\sqrt{4Z_{wb}^2+h_D^2(1-\rho^2)}} \tag{19}$$

If $\rho=1$ this expression simplifies to $\tan\gamma=\frac{h_D}{2Z_{wb}}$, which is the aperture angle of a primary at twice the water-bottom depth. As we did with the SODCIG, it is important to find the

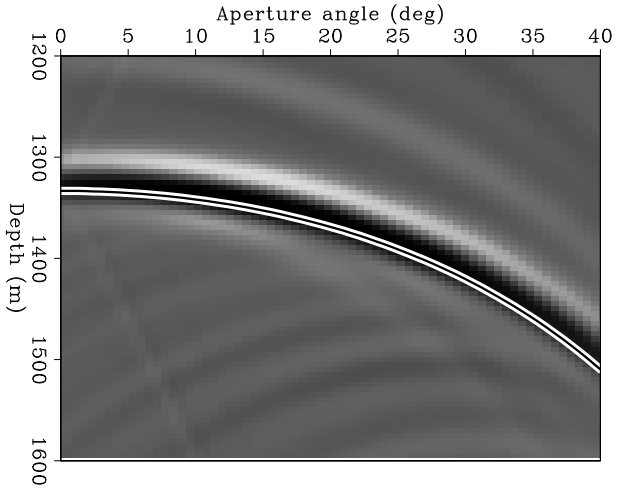

Figure 6: Angle domain common image gather corresponding to the SODCIG shown in Figure 5. Overlaid is the residual moveout curve computed with equation 20. gabriel1-adcig1 [CR]

functional relationship between z_{ξ_γ} and γ since it dictates the residual moveout of the multiple in the ADCIG. Plugging Equations 14 and 15 into equation 12, using Equations 13, and 18 to eliminate h_D and simplifying we get

$$z_{\xi_\gamma}=Z_{wb}\left[1+\frac{\cos\gamma(\rho^2-\tan^2\gamma(1-\rho^2))}{\sqrt{\rho^2-\sin^2\gamma}}\right]=\frac{z_{\xi_\gamma}(0)}{1+\rho}\left[1+\frac{\cos\gamma(\rho^2-\tan^2\gamma(1-\rho^2))}{\sqrt{\rho^2-\sin^2\gamma}}\right]. \tag{20}$$

Once again, when the multiple is migrated with the water velocity ($\rho=1$) we get the expected result $z_{\xi_\gamma}=z_{\xi_\gamma}(0)$, that is, flat moveout (no angular dependence). Figure 6 shows the ADCIG corresponding to the SODCIG shown in Figure 5. Notice that the migrated depth at zero aperture angle is the same as that for zero sub-surface offset in Figure 5. For larger aperture angles, however, the migrated depth increases as indicated in equation 20 and as seen in the schematic of Figure 4.

Diffracted multiple

Consider now a diffractor sitting at the water-bottom as illustrated in the sketch in Figure 7. The source- and receiver-side multiples are described by equations 2–4 as did the water-bottom

multiple. In this case, however, the take-off angles from source and receiver are different even if the surface offset is the same as that in Figure 4. In fact, since the reflection is non-specular at the location of the diffractor, X_{diff} needs to be known in order for the receiver take-off angle to be computed. The traveltime of the diffracted multiple is given by

$$t_m = \frac{1}{V_1}\left[3\sqrt{Z_{wb}^2 + \left[\frac{X_{diff} - (m_D - h_D)}{3}\right]^2} + \sqrt{\left[(m_D + h_D) - X_{diff}\right]^2 + Z_{wb}^2}\right], \qquad (21)$$

where $Z_{wb} = Z_{diff}$ can be computed from the traveltime of the multiple for the zero subsurface offset trace ($t_m(0)$) by solving the quadratic equation in Z_{wb}^2 that results from setting $h_D = 0$ in equation 21:

$$64Z_{wb}^4 - 20V_1^2 t_m^2(0) Z_{wb}^2 + (V_1^4 t_m^4(0) - 4V_1^2 t_m^2(0)(m_D - X_{diff})^2) = 0 \qquad (22)$$

The coordinates of the image point, according to equations 2–4 are given by

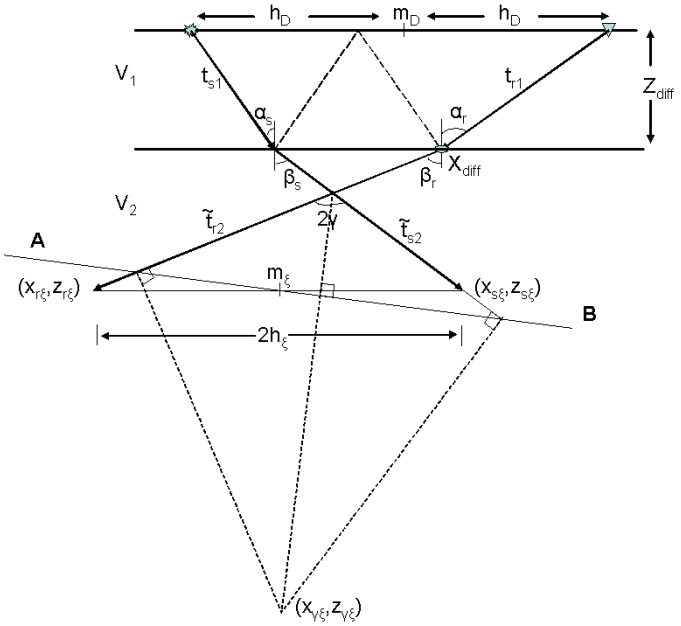

Figure 7: Imaging of receiver-side diffracted water-bottom multiple from a diffractor sitting on top of a flat water-bottom. At the diffractor the reflection is non-specular. Notice that $m_D \neq m_\xi$. gabriel1-mul_sktch5 [NR]

$$h_\xi = h_D - \frac{V_1}{2}\left[t_{s_1}\sin\alpha_s + t_{r_1}\sin\alpha_r + \rho^2(\tilde{t}_{s_2}\sin\alpha_s + \tilde{t}_{r_2}\sin\alpha_r)\right], \qquad (23)$$

$$z_\xi = Z_{wb} + \rho V_1 \tilde{t}_{r_2}\cos\beta_r, \qquad (24)$$

$$m_\xi = m_D + \frac{V_1}{2}(t_{s_1}\sin\alpha_s - t_{r_1}\sin\alpha_r + \rho^2(\tilde{t}_{s_2}\sin\alpha_s - \tilde{t}_{r_2}\sin\alpha_r)). \qquad (25)$$

The traveltimes of the individual ray segments are given by

$$t_{s_1} = t_{s_2} = t_{r_2} = \frac{X_{diff} - (m_D - h_D)}{3V_1\sin\alpha_s}, \quad \text{and} \quad t_{r_1} = \frac{m_D + h_D - X_{diff}}{V_1\sin\alpha_r}, \qquad (26)$$

whereas the traveltimes of the refracted rays can be computed from equation 5:

$$\tilde{t}_{s_2} = \frac{t_{s_2}(2\rho\cos\beta_r - \cos\alpha_s) + t_{r_1}\cos\alpha_r}{\rho(\cos\beta_r + \cos\beta_s)}, \quad \text{and} \quad \tilde{t}_{r_2} = \frac{t_{s_2}(2\rho\cos\beta_s + \cos\alpha_s) - t_{r_1}\cos\alpha_r}{\rho(\cos\beta_r + \cos\beta_s)}. \tag{27}$$

where, according to equations 9 and 10:

$$\cos\beta_s = \sqrt{1-\rho^2\sin^2\alpha_s} \quad \text{and} \quad \cos\beta_r = \sqrt{1-\rho^2\sin^2\alpha_r}. \tag{28}$$

In order to express h_ξ, z_ξ and m_ξ entirely in terms of the data space coordinates, all we need to do is compute the sines and cosines of α_s and α_r which can be easily done from the sketch of Figure 7:

$$\sin\alpha_s = \frac{X_{diff} - (m_D - h_D)}{3\sqrt{((X_{diff} - (m_D - h_D))/3)^2 + Z_{wb}^2}} \qquad \cos\alpha_s = \frac{Z_{wb}}{\sqrt{((X_{diff} - (m_D - h_D))/3)^2 + Z_{wb}^2}}$$

$$\sin\alpha_r = \frac{(m_D + h_D) - X_{diff}}{\sqrt{((m_D + h_D) - X_{diff})^2 + Z_{wb}^2}} \qquad \cos\alpha_r = \frac{Z_{wb}}{\sqrt{((m_D + h_D) - X_{diff})^2 + Z_{wb}^2}}$$

Notice that the diffraction multiple does not migrate as a primary even if migrated with water velocity. In other words, even if $\rho = 1$, $h_\xi \neq 0$. The only exception is when $X_{diff} = m_D + h_D/2$ since then the diffractor is in the right place to make a specular reflection and therefore is indistinguishable from a non-diffracted water-bottom multiple. In that case, $\alpha_r = \alpha_s$ (which in turn implies $\beta_r = \beta_s$) and from equations 5 and 6, $\tilde{t}_{r_2} = \tilde{t}_{s_2} = t_{s_2}$ and therefore equations 23–25 reduce to equations 14–16, respectively. Figure 8 shows two subsurface-offset sections

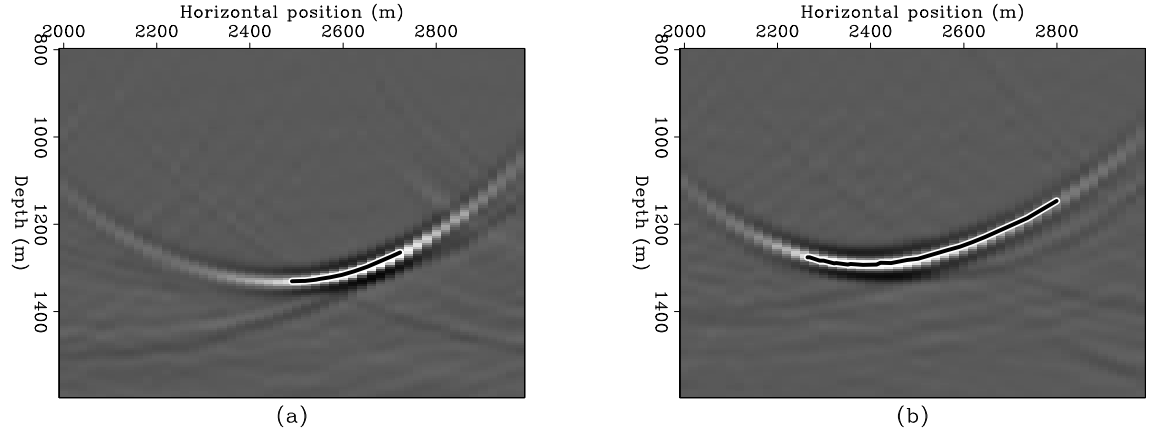

Figure 8: image sections at 0 and -400 m subsurface offset for a diffracted multiple from a flat water-bottom. The depth of the water-bottom is 500 m and the diffractor is located at 2500 m. The solid line represents image reflector computed with equations 24 and 25. gabriel1-image2 [CR]

of a migrated diffracted multiple from a diffractor sitting on top of a flat reflector as in the

schematic of Figure 7. The diffractor position is $X_{diff} = 2{,}500$ m, the CMP range is from 2,000 m to 3,000 m, the offsets range from 0 to 2,000 m and the water depth is 500 m. The data were migrated with the same two-layer model described before. Panel (a) corresponds to zero subsurface offset ($h_\xi = 0$) whereas panel (b) corresponds to subsurface offset of -400 m. Overlaid are the residual moveout curves computed with equations 24 and 25. Obviously, the zero subsurface offset section is not a good image of the water-bottom or the diffractor.

Figure 9 shows three SODCIGs taken at locations 2,300 m, 2,500 m and 2,700 m. Unlike the non-diffracted multiple, this time energy maps to positive or negative subsurface offset depending on the relative position of the CMP with respect to the diffractor. In ADCIGs the aperture angle is given by equation 11 which, given the geometry of Figure 7, reduces to

$$\gamma = \frac{1}{2}\sin^{-1}[\beta_s + \beta_r] = \frac{1}{2}\sin^{-1}\left[\rho\sin\alpha_r\sqrt{1-\rho^2\sin^2\alpha_s} + \rho\sin\alpha_s\sqrt{1-\rho^2\sin^2\alpha_r}\right]. \quad (29)$$

The depth of the image is given by equation 12,

$$z_{\xi_\gamma} = z_\xi - h_\xi\tan\left(\frac{1}{2}\sin^{-1}\left[\rho\sin\alpha_r\sqrt{1-\rho^2\sin^2\alpha_s} + \rho\sin\alpha_s\sqrt{1-\rho^2\sin^2\alpha_r}\right]\right). \quad (30)$$

Again, this equation shows that the diffracted multiple is not migrated as a primary even if

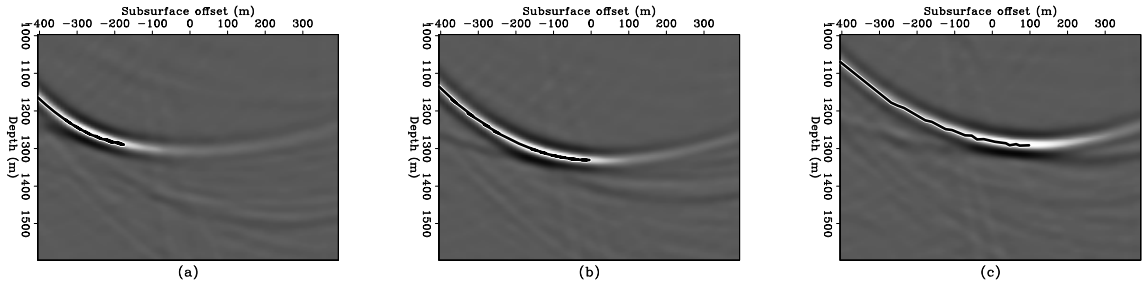

Figure 9: SODCIGs from a diffracted multiple from a flat water-bottom at locations 2,300 m, 2,500 m and 2,700 m. The diffractor is at 2,500 m. The overlaid residual moveout curves were computed with equations 23 and 24. gabriel1-odcig2 [CR]

$\rho = 1$ (except in the trivial case $X_{diff} = m_D + h_D/2$ discussed before for which, since $\alpha_r = \alpha_s$, $\gamma = \beta_s = \beta_r$ in agreement with equation 19 and so equation 30 reduces to equation 20). Figure 10 shows the angle gathers corresponding to the SODCIGs of Figure 9. Notice the shift in the apex of the moveout curves.

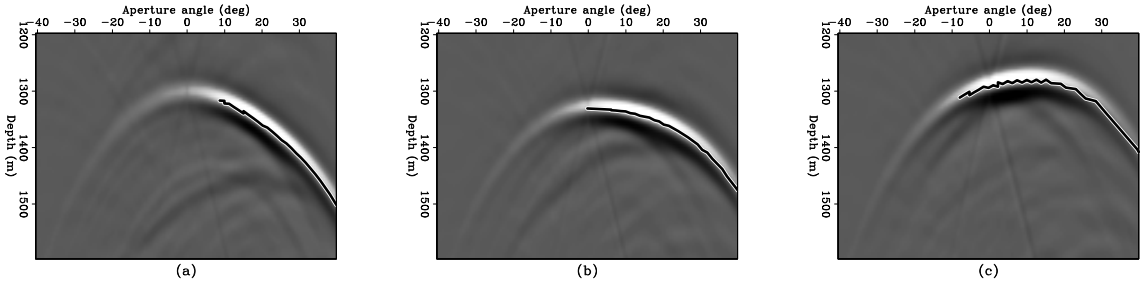

Figure 10: ADCIGs corresponding to the SODCIGs in Figure 9. The overlaid curves are the residual moveout curves computed with equations 24 and 30. gabriel1-adcig2 [CR]

DIPPING WATER-BOTTOM

Water-bottom multiple

The water-bottom multiple from a dipping reflector has exactly the same kinematics as a primary from a reflector with twice the dip (Alvarez, 2005), that is,

$$t_m = \sqrt{\left(\frac{2\hat{Z}_D}{V_1}\right)^2 + \left(\frac{2h_D}{\hat{V}_{NMO}}\right)^2} = \sqrt{t_m^2(0) + \left(\frac{2h_D}{\hat{V}_{NMO}}\right)^2}, \tag{31}$$

where φ is the dip of the reflector, $\hat{Z}_D$ is the perpendicular depth to the equivalent reflector with twice the dip (at the CMP location) and $\hat{V}_{NMO}$ is the NMO velocity of the equivalent primary $\hat{V}_{NMO} = V_1/\cos(2\varphi)$.

Following the same procedure as for the flat water-bottom, we compute the coordinates of the image point using equations 2–4 and noting that in this case $\alpha_r = \alpha_s + 4\varphi$,

$$\begin{aligned}
h_\xi &= h_D - \frac{V_1}{2}\left[t_{s_1}\sin\alpha_s + t_{r_1}\sin(\alpha_s+4\varphi) + \rho\left(\tilde{t}_{s_2}\sin\beta_s + \tilde{t}_{r_2}\sin\beta_r\right)\right], && (32)\\
z_\xi &= V_1\left(t_{r_1}\cos\alpha_s + \rho\tilde{t}_{s_2}\left[\sqrt{1-\rho^2\sin^2(\alpha_s+\varphi)}\cos\varphi + \rho\sin(\alpha_s+\varphi)\sin\varphi\right]\right), && (33)\\
m_\xi &= m_D + \frac{V_1}{2}(t_{s_1}\sin\alpha_s - t_{r_1}\sin(\alpha_s+4\varphi) + \rho(\tilde{t}_{s_2}\sin\beta_s - \tilde{t}_{r_2}\sin\beta_r)). && (34)
\end{aligned}$$

where, according to equations 7–10,

$$\begin{aligned}
\sin\beta_s &= \rho\sin(\alpha_s+\varphi)\cos\varphi - \sqrt{1-\rho^2\sin^2(\alpha_s+\varphi)}\sin\varphi, && (35)\\
\sin\beta_r &= \rho\sin(\alpha_s+3\varphi)\cos\varphi + \sqrt{1-\rho^2\sin^2(\alpha_s+3\varphi)}\sin\varphi, && (36)\\
\cos\beta_s &= \sqrt{1-\rho^2\sin^2(\alpha_s+\varphi)}\cos\varphi + \rho\sin(\alpha_s+\varphi)\sin\varphi, && (37)\\
\cos\beta_r &= \sqrt{1-\rho^2\sin^2(\alpha_s+3\varphi)}\cos\varphi - \rho\sin(\alpha_s+3\varphi)\sin\varphi. && (38)
\end{aligned}$$

The traveltimes of the individual ray segments are computed by repeated application of the law of sines as shown in Appendix C:

$$t_{s_1} = \frac{\tilde{Z}_s}{V_1\cos(\alpha_s+\varphi)} = \frac{\tilde{Z}_D - h_D\sin\varphi}{V_1\cos(\alpha_s+\varphi)}, \tag{39}$$

$$t_{s_2} = \frac{t_{s_1}\cos\alpha_s}{\cos(\alpha_s+2\varphi)} = \frac{(\tilde{Z}_D - h_D\sin\varphi)\cos\alpha_s}{V_1\cos(\alpha_s+\varphi)\cos(\alpha_s+2\varphi)}, \tag{40}$$

$$t_{r_2} = \frac{t_{s_2}\cos(\alpha_s+\varphi)}{\cos(\alpha_s+3\varphi)} = \frac{(\tilde{Z}_D - h_D\sin\varphi)\cos\alpha_s}{V_1\cos(\alpha_s+2\varphi)\cos(\alpha_s+3\varphi)}, \tag{41}$$

$$t_{r_1} = \frac{t_{r_2}\cos(\alpha_s+2\varphi)}{\cos(\alpha_s+4\varphi)} = \frac{(\tilde{Z}_D - h_D\sin\varphi)\cos\alpha_s}{V_1\cos(\alpha_s+3\varphi)\cos(\alpha_s+4\varphi)}, \tag{42}$$

where $\tilde{Z}_D$ is the perpendicular depth to the reflector at the CMP location and is given by (Appendix C):

$$\tilde{Z}_D = \frac{V_1 t_m(0)\cos\varphi}{2[1+\cos(2\varphi)]}. \tag{43}$$

Notice that this is not the same as $\hat{Z}_D$ in equation 31, which corresponds to the perpendicular depth to the equivalent reflector whose primary has the same kinematics as the water-bottom multiple.

The traveltime of the refracted ray segments are given by equations 5 and 6 with

$$\cos\alpha_r = \sqrt{1-\sin^2(\alpha_s+4\varphi)}, \quad \text{and} \quad \cos\alpha_s = \sqrt{1-\sin^2\alpha_s}. \tag{44}$$

In order for equation 32–34 to be useful in practice, we need to express them entirely in terms of the known data coordinates, which means that we need to find an expression for α_s in terms of (t_m, h_D, m_D, φ). In Appendix C it is shown that

$$\alpha_s = \sin^{-1}\left[\frac{2h_D\cos(2\varphi)}{V_1 t_m}\right] - 2\varphi. \tag{45}$$

We now have all the pieces to compute the image space coordinates, since $\tilde{t}_{s_2}$ and $\tilde{t}_{r_2}$ can be computed from equations 5 and 6 using equations 35–45.

Appendix D shows that equations 32–34 reduce to the corresponding equations for the non-diffracted multiple from a flat water bottom when $\varphi = 0$, as they should.

Figure 11 shows the zero subsurface offset section from a migrated non-diffracted multiple from a dipping water-bottom. The overlaid curve was computed with equations 32–34. The dip of the water-bottom is 15 degrees and intercepts the surface at CMP location zero. The CMP range of the data is from 2000 to 3000 m and the surface offsets from 0 to 2000 m. The multiple was migrated with the same two-layer model described before. Notice how the multiple was migrated as a primary. Since the migration velocity is faster than water-velocity, the multiple is over-migrated and appears much steeper and shallower than it should (recall that it would be migrated as a reflector with twice the dip is the migration velocity were that

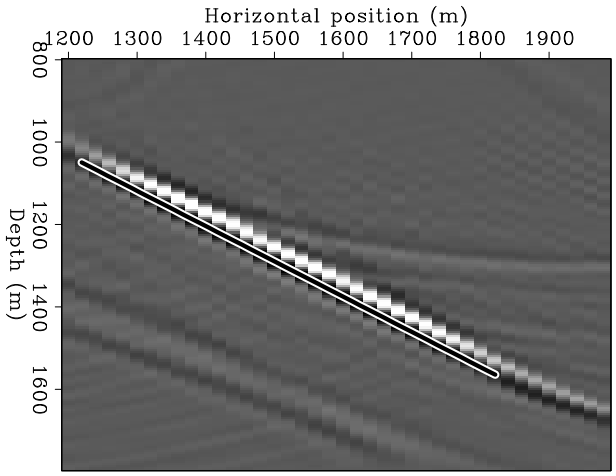

Figure 11: image section at zero subsurface offset for a non-diffracted multiple from a dipping water-bottom. The overlaid curve was computed with equation 34 and 33. gabriel1-image3 [CR]

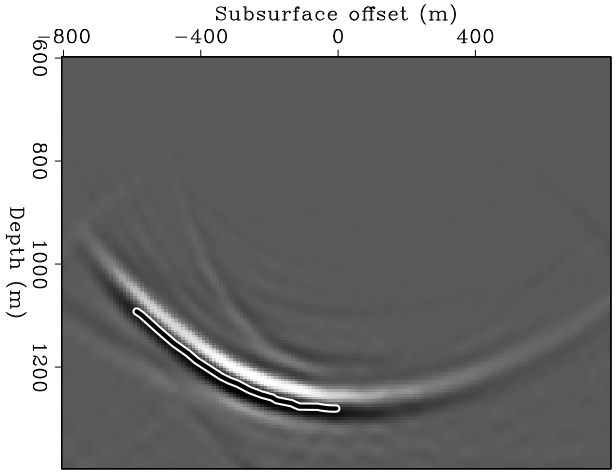

Figure 12: SODCIG from a non-diffracted multiple from a dipping water-bottom. The overlaid residual moveout curve was computed with equation 32 and 33. gabriel1-odcig3 [CR]

of the water.) Figure 12 shows the SODCIG at CMP 1500 m in i Figure 11. Just as for the flat water-bottom, the multiple energy is mapped to negative subsurface offsets since $\rho > 1$. The overlaid curve is the moveout computed with equations 32–34. The aperture angle is given by equation 11 with

$$\beta_r = \sin^{-1}(\rho \sin(\alpha_s + 3\varphi)) - \varphi \quad \text{and} \quad \beta_s = \sin^{-1}(\rho \sin(\alpha_s + \varphi)) - \varphi \tag{46}$$

and α_s given by equation 45. The image depth in the ADCIG is given by equation 12 with β_s and β_r given by equation 46 and h_ξ and z_ξ given by equations 32 and 33. Figure 13 shows the ADCIG corresponding to the SODCIG in Figure 12. Notice that the apex is at zero aperture angle.

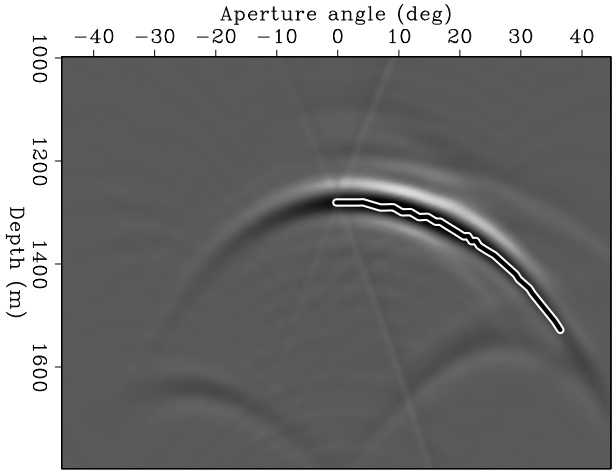

Figure 13: ADCIG corresponding to the SODCIG shown in Figure 12. The overlaid residual moveout curve was computed with equation 33, 11, 12, and 46. gabriel1-adcig3 [CR]

Diffracted multiple

Figure 14 shows the raypath of a diffracted multiple from a dipping reflector. The image-space coordinates of the diffracted multiple are given by the same equations as the water-bottom multiple, *i.e.* equations 32–34. The main difference is that now $\alpha_r \neq \alpha_s + 4\varphi$. In fact, α_r depends exclusively oh the position of the diffractor with respect to the receiver and is given by (Appendix E)

$$\alpha_r = \tan^{-1}\left[\frac{h_D + m_D - X_{diff}}{Z_{diff}}\right]. \tag{47}$$

The depth of the diffractor Z_{diff} can be computed as (Appendix E):

$$Z_{diff} = \tilde{Z}_D \cos\varphi + (X_{diff} - m_D)\tan\varphi, \tag{48}$$

where $\tilde{Z}_D$, as before, is the perpendicular distance between the CMP and the reflector. It can be computed from the traveltime of the diffracted multiple of the zero surface-offset trace as shown in Appendix E. The traveltime segments from the source to the diffractor are the same

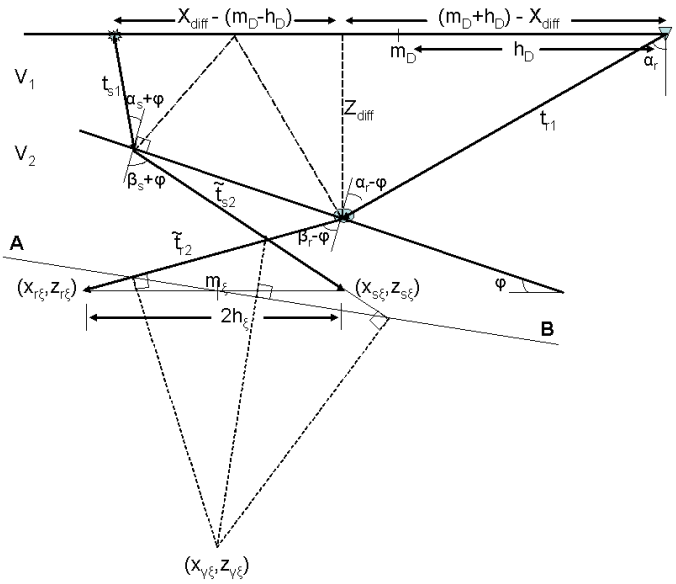

Figure 14: Diffracted multiple from a dipping water-bottom. Note that the receiver ray does not satisfy Snell's law at the diffractor. gabriel1-mul_sktch6 [NR]

as before and given by equations 39–41, while the traveltime from the diffractor to the receiver is simply

$$t_{r_1} = \frac{1}{V_1}\sqrt{(h_D + (m_D - X_{diff}))^2 + Z_{diff}^2}. \tag{49}$$

In order to have the image coordinates entirely in terms of the data space coordinates all that is left is to compute α_s (Appendix E):

$$\alpha_s = \sin^{-1}\left[\frac{2\tilde{Z}_D \sin\varphi + (h_D + X_{diff} - m_D)}{V_1 t_m - \sqrt{(h_D + m_D - X_{diff})^2 + Z_{diff}^2}}\right] - 2\varphi. \tag{50}$$

Figure 15 shows three image sections at subsurface offsets of 0, -200 and 200 m. These

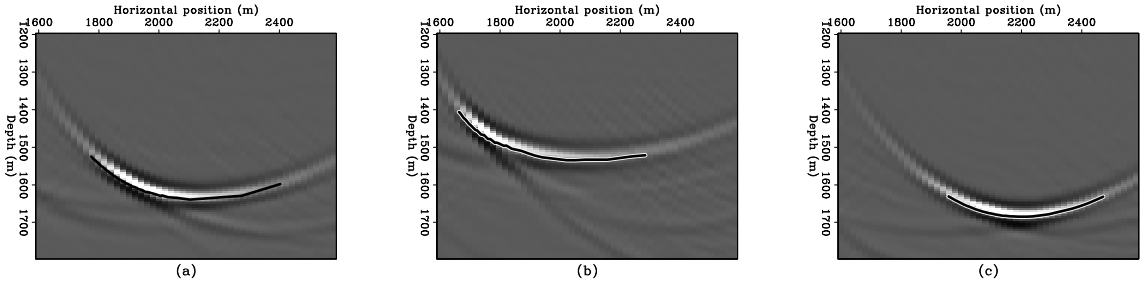

Figure 15: image sections at 0, -200 and 200 m subsurface offset for a diffracted multiple from a dipping water-bottom. gabriel1-image4 [CR]

sections are a poor representation of either the reflector or the diffractor since the diffracted multiple is not imaged as a primary. Figure 16 shows three SODCIGs at CMP locations 1800, 2200 and 2600 m. Again, we see that the SODCIGs are very different depending on their

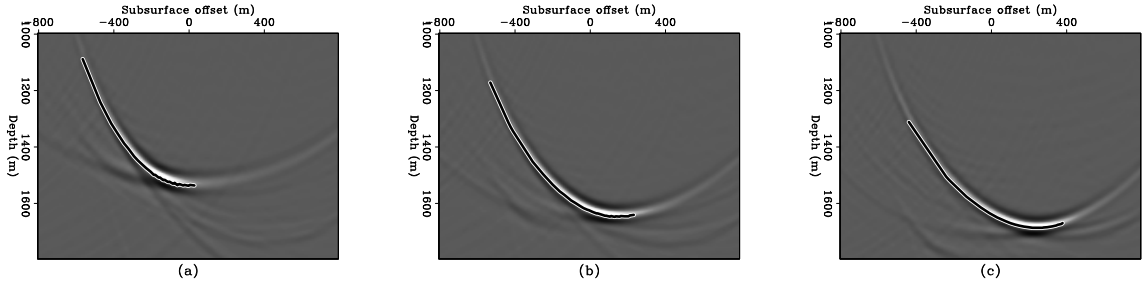

Figure 16: SODCIGs at three different CMP locations: 1,800, 2,000 and 2,200 m for a diffracted multiple from a dipping water-bottom. gabriel1-odcig4 [CR]

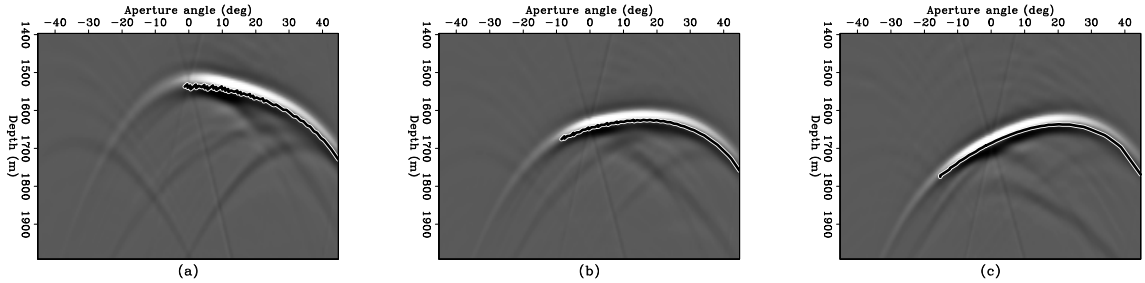

Figure 17: ADCIGs corresponding to the three SODCIGs of Figure 16. gabriel1-adcig4 [CR]

relative position to the diffractor, unlike the situation with the non-diffracted multiple which maps to negative subsurface offsets (for $h_D \geq 0$) for all SODCIGs. The aperture angle and the image depth of the diffracted multiple in ADCIGs can also be computed with equations 11 and 12 with β_r and β_s given by equation 46. Figure 17 shows the ADCIG corresponding to the same ODCIG in Figure 16. Again, notice that the apex is shifted away from zero aperture angle.

DISCUSSION

The results of the previous sections illustrate that non-diffracted water-bottom multiples (whether from flat or dipping water-bottom) map to negative subsurface offsets (since $h_D \geq 0$ in this case), whereas primaries migrated with slower velocities would map to positive subsurface offsets. This suggests an easy strategy to attenuate these multiples. Migrate the data with a constant velocity that is faster than water velocity but slower than sediment velocity. Keep only the positive subsurface offsets and demigrate with the same velocity. In principle, the primaries would be restored (at least kinematically) whereas the multiples would be attenuated. Although not shown here, the same conclusion can be reached for higher-order non-diffracted water-bottom multiples. This strategy, however, would not work for diffracted multiples since they may map to positive subsurface offsets even when migrated with a velocity faster than water velocity as illustrated schematically in Figure 18. We can still separate these multiples from the primaries, but that requires the application of an appropriate Radon transform. An

apex-shifted tangent-squared Radon transform was applied by Alvarez et. al. (2004) to a real 2D section with good results, but the basic assumption there was that of no ray-bending at the water-bottom interface. It is expected that the more accurate equations derived here will allow the design of a better Radon transform and therefore a better degree of separation between primaries and diffracted multiples. This is the subject of continuing research. For the non-diffracted multiple from a flat water-bottom the mapping between the image-space coordinates and the data-space coordinates is essentially 2D since $m_D = m\xi$, which allowed the computation of closed-form expressions for the residual moveout of the multiples in both SODCIGs and ADCIGs. For diffracted multiples in particular, it is not easy to compute equivalent closed-form expressions, but we can compute numerically the residual moveout curves given the expression for (h_ξ, z_ξ, m_ξ) in terms of the data-space coordinates (t_m, h_D, m_D), φ and X_{diff}. In principle, the dip of the water-bottom can be estimated from the data and the position of the diffractor corresponds to the lateral position of the apex of the multiple diffraction in a shot gather as illustrated in the sketch of Figure 19.

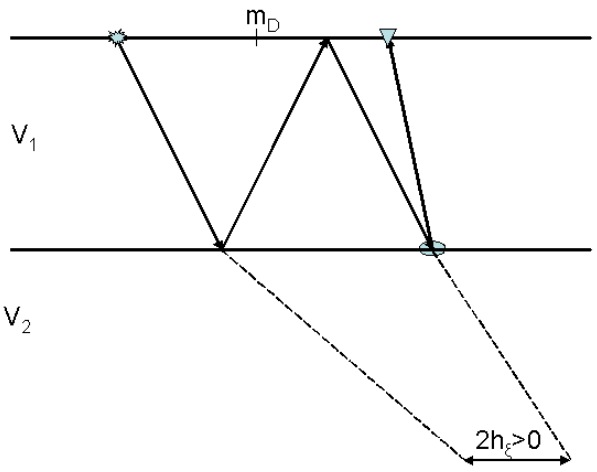

Figure 18: Sketch illustrating that diffracted multiples may map to positive subsurface offsets. gabriel1-mul_sktch7 [NR]

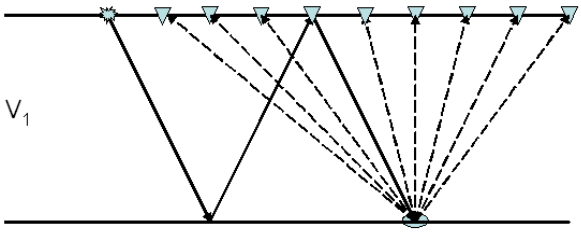

Figure 19: Sketch illustrating the raypaths of a diffracted multiple in a shot gather. The lateral position of the diffractor corresponds to the apex of the moveout curve. gabriel1-mul_sktch8 [NR]

CONCLUSIONS

Non-diffracted water-bottom multiples, whether from a flat or dipping water-bottom, map to zero or negative subsurface offsets when migrated with the velocity of the sediments $\rho > 1$ for $h_D \geq 0$. On the other hand, primaries migrated with slower velocities map to positive subsurface offsets. It may be possible to exploit this fact to attenuate these multiples.

Diffracted water-bottom multiples, in contrast, map to both positive and negative subsurface offsets depending on the relative position of the CMP and the diffractor. To attenuate these multiples we need an accurate representation of their residual moveouts in either SODCIGs or ADCIGs as presented here to design a suitable Radon transform that focuses these multiples to predictable locations in the Radon domain. This is the subject of ongoing research.

REFERENCES

Alvarez, G., Biondi, B., and Guitton, A., 2004, Attenuation of diffracted multiples in angle-domain common-image gathers:, *in* 74th Ann. Internat. Mtg. Soc. of Expl. Geophys., 1301–1304.

Alvarez, G., 2005, Water-bottom and diffracted 2D multiple reflections in data space and image space: SEP–**120**, 363–374.

Biondi, B., and Symes, W., 2004, Angle-domain common-image gathers for migration velocity analysis by wavefield-continuation imaging: Angle-domain common-image gathers for migration velocity analysis by wavefield-continuation imaging:, Soc. of Expl. Geophys., Geophysics, 1283–1298.

Hargreaves, N., Wombell, R., and West, B. V., 2003, Multiple attenuation using an apex-shifted radon transform: 65th Conference and Exhibition, EAEG, Strategies towards multi-dimensional multiple attenuation.

Rosales, D. A., and Biondi, B., 2005, Converted-mode angle-domain common-image gathers for migration velocity analysis: SEP–**120**, 283–296.

Sava, P., and Guitton, A., 2003, Multiple attenuation in the image space: SEP–**113**, 31–44.

APPENDIX A

COMPUTATION OF TRAVELTIME FOR REFRACTED RAYS

In this Appendix I derive equations 5 and 6. From equation 3 we have:

$$t_{s_1}\cos\alpha_s + \rho\tilde{t}_{s_2}\cos\beta_s = t_{r_1}\cos\alpha_r + \rho\tilde{t}_{r_2}\cos\beta_r, \tag{A-1}$$

and, from the condition that the sum of the traveltime of the extrapolated rays at the image point has to be equal to the traveltime of the multiple we have

$$t_{s_2} + t_{r_2} = \tilde{t}_{s_2} + \tilde{t}_{r_2}. \tag{A-2}$$

Solving those two equations for $\tilde{t}_{s_2}$ and $\tilde{t}_{r_2}$ we get

$$\tilde{t}_{s_2} = \frac{t_{r_1}\cos\alpha_r - t_{s_1}\cos\alpha_s + \rho(t_{s_2}+t_{r_2})\cos\beta_r}{\rho(\cos\beta_s+\cos\beta_r)}, \quad \text{(A-3)}$$

$$\tilde{t}_{r_2} = \frac{t_{s_1}\cos\alpha_s - t_{r_1}\cos\alpha_r + \rho(t_{s_2}+t_{r_2})\cos\beta_s}{\rho(\cos\beta_s+\cos\beta_r)}. \quad \text{(A-4)}$$

It is interesting to check these equations in two particular cases. For a non-diffracted flat water-bottom multiple, we have $\alpha_s = \alpha_r$, $\beta_s = \beta_r$, $t_{s_1} = t_{s_2} = t_{r_2} = t_{r_1}$ and therefore we get $\tilde{t}_{s_2} = t_{s_2}$ and $\tilde{t}_{r_2} = t_{r_2}$ as the geometry of the problem requires. Notice that this is true for any ρ. The second case is for a non-diffracted water-bottom multiple migrated with water velocity. In that case, $\beta_s = \alpha_s$ and $\beta_r = \alpha_r$. Furthermore, since the multiple behaves as a primary, $(t_{s_1}+t_{s_2})\cos\alpha_s = (t_{r_1}+t_{r_2})\cos\alpha_r$ and we again get $\tilde{t}_{s_2} = t_{s_2}$ and $\tilde{t}_{r_2} = t_{r_2}$.

APPENDIX B

COMPUTATION OF IMAGE DEPTH IN ADCIGS

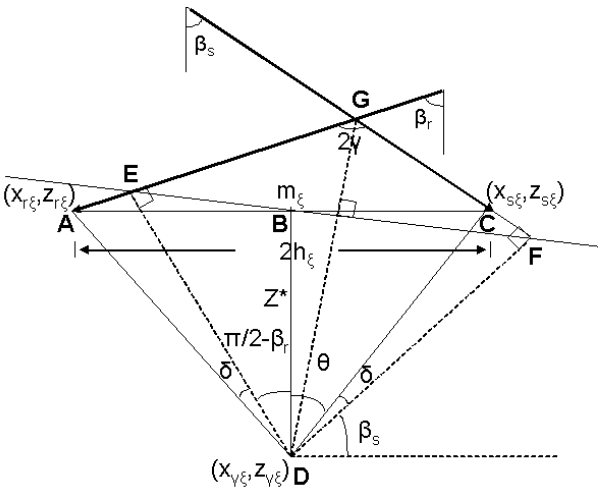

Figure B-1: Sketch to show the computation of the image depth in an ADCIG. gabriel1-mul_sktch17 [NR]

Figure B-1 shows the basic construction to compute the image depth in ADCIGs based on the image depth is SOCIGs. Triangles ABD and CBD are congruent since they have one side common and the other equal because |AB|=|BC|=h_ξ. Therefore, $\theta = \pi/2 - \beta_r + \delta$. Also, triangles AED and FCD are congruent because |AD|=|CD| and also |AE|=|CF| (Biondi and Symes, 2004). Therefore, the angle δ in triangle DCF is the same as in triangle AED. We can compute δ from the condition

$$\begin{aligned} \theta + \delta + \beta_s &= \frac{\pi}{2}, \\ \frac{\pi}{2} - \beta_r + \delta + \delta + \beta_s &= \frac{\pi}{2}, \\ \delta &= \frac{\beta_r - \beta_s}{2}. \end{aligned}$$

The depth of the image point in the ADCIG, from triangle ABC, is therefore

$$z_{\xi_\gamma} = z_\xi + z^* = z_\xi + (\text{sign}(h_\xi))h_\xi \cot\left(\frac{\pi}{2} - \beta_r + \delta\right). \tag{B-1}$$

Replacing the expression for δ we get, after some simplification (and taking $\text{sign}(h_\xi) = -1$)

$$z_{\xi_\gamma} = z_\xi + z^* = z_\xi - h_\xi \tan\left(\frac{\beta_r + \beta_s}{2}\right) = z_\xi - h_\xi \tan(\gamma). \tag{B-2}$$

APPENDIX C

TRAVELTIME COMPUTATIONS FOR DIPPING WATER-BOTTOM MULTIPLE

In this Appendix I derive equations 39–45. From triangle ABC in Figure C-1 we immediately get

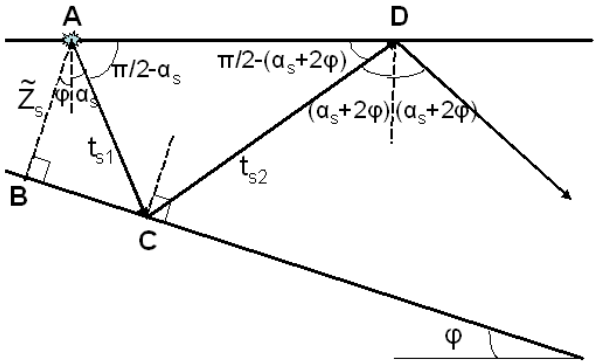

Figure C-1: Sketch to show the computation of t_{s_1} and t_{s_2} for a non-diffracted multiple from a dipping water-bottom. gabriel1-mul_sktch9 [NR]

$$t_{s_1} = \frac{\tilde{Z}_s}{\cos(\alpha_s + \varphi)} \tag{C-1}$$

and applying the law of sines to triangle ACD we get

$$t_{s_2} = \frac{t_{s_1}\cos\alpha_s}{\cos(\alpha_s + 2\varphi)} = \frac{\tilde{Z}_s \cos\alpha_s}{V_1 \cos(\alpha_s + \varphi)\cos(\alpha_s + 2\varphi)}. \tag{C-2}$$

Similarly, repeated application of the law of sines to triangles CDE and DEF in Figure C-2 gives

$$t_{r_2} = \frac{t_{s_2}\cos(\alpha_s + \varphi)}{\cos(\alpha_s + 3\varphi)} = \frac{\tilde{Z}_s \cos\alpha_s}{V_1 \cos(\alpha_s + 2\varphi)\cos(\alpha_s + 3\varphi)} \tag{C-3}$$

$$t_{r_1} = \frac{t_{r_2}\cos(\alpha_s + 2\varphi)}{\cos(\alpha_s + 4\varphi)} = \frac{\tilde{Z}_s \cos\alpha_s}{V_1 \cos(\alpha_s + 3\varphi)\cos(\alpha_s + 4\varphi)}. \tag{C-4}$$

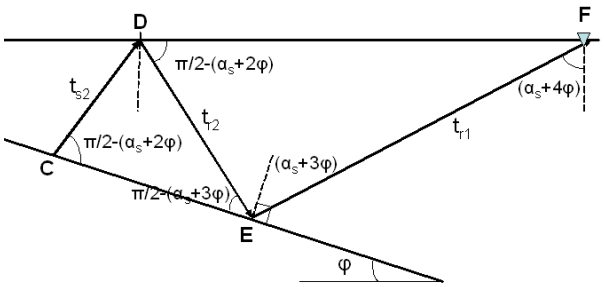

Figure C-2: Sketch to show the computation of t_{r_2} and t_{r_1} for a non-diffracted multiple from a dipping water-bottom. gabriel1-mul_sktch10 [NR]

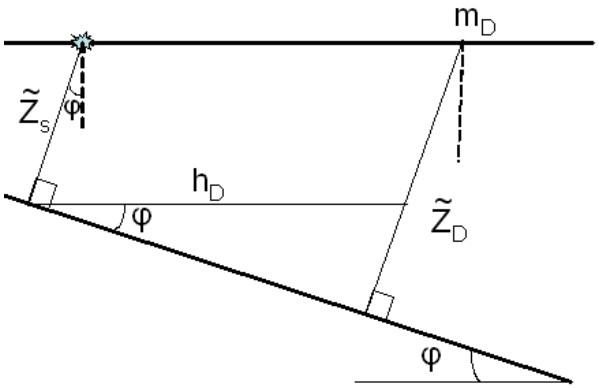

Figure C-3: Sketch to show the computation of $\tilde{Z}_s$ in equation C-5. gabriel1-mul_sktch11 [NR]

These equations are in terms of $\tilde{Z}_s$, which is not known. However, from Figure C-3 we see that

$$\tilde{Z}_s = \tilde{Z}_D - h_D \sin\varphi, \tag{C-5}$$

and $\tilde{Z}_D$ can be computed from the traveltime of the zero surface-offset trace, since, according to Figure C-4

$$t_m(0) = \frac{2\tilde{Z}_D}{V_1\cos\varphi} + \frac{2\tilde{Z}_D\cos(2\varphi)}{V_1\cos\varphi} = \frac{2\tilde{Z}_D(1+\cos(2\varphi))}{V_1\cos\varphi}, \tag{C-6}$$

from which it follows immediately that

$$\tilde{Z}_D = \frac{V_1 t_m(0)\cos\varphi}{2[1+\cos(2\varphi)]}. \tag{C-7}$$

Finally, we need to compute α_s. Applying the law of sines to triangle ABC in Figure C-5 we get

$$\sin(\alpha_s + 2\varphi) = \frac{2h_D\cos(2\varphi)}{V_1 t_m}, \tag{C-8}$$

from which we get

$$\alpha_s = \sin^{-1}\left[\frac{2h_D\cos(2\varphi)}{V_1 t_m}\right] - 2\varphi. \tag{C-9}$$

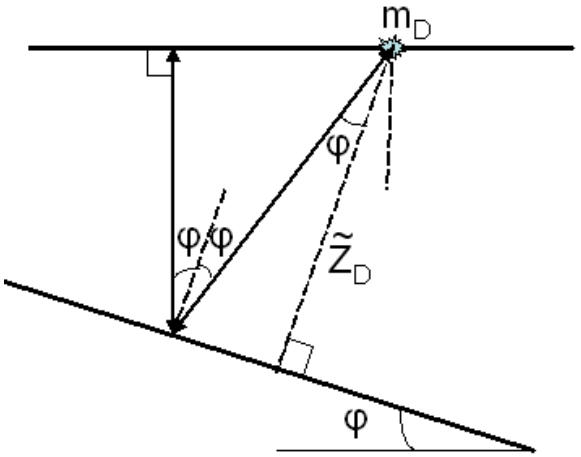

Figure C-4: Sketch to show the computation of $\tilde{Z}_D$ in equation C-7. gabriel1-mul_sktch12 [NR]

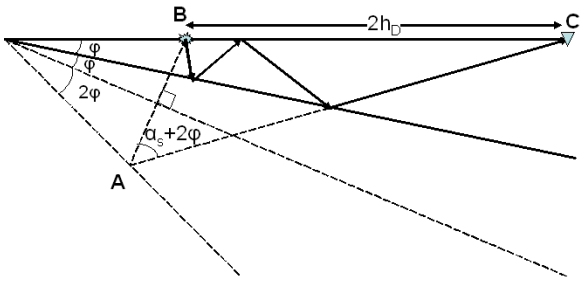

Figure C-5: Sketch to compute the takeoff angle of the source ray from a non-diffracted multiple from a dipping water-bottom. gabriel1-mul_sktch16 [NR]

APPENDIX D

FROM DIP TO NO DIP FOR NON-DIFFRACTED MULTIPLE

In this Appendix, I show that the equations for the non-diffracted multiple from a dipping water-bottom reduce to the equations for a flat water-bottom when $\varphi = 0$ as they should. Setting $\varphi = 0$ in equations 39 through 42 we obtain

$$t_{s_2} = t_{r_2} = t_{r_1} = t_{s_1} = \frac{\tilde{Z}_s}{\cos\alpha_s} \tag{D-1}$$

and from equations 5 and 6 we get (as discussed at the end of Appendix A) $\tilde{t}_{r_2} = t_{r_2}$ and $\tilde{t}_{s_2} = t_{s_2}$. Therefore,

$$\begin{aligned} h_\xi &= 2h_D - V_1[t_{s_1}\sin\alpha_s + t_{r_1}\sin\alpha_r + \rho(\tilde{t}_{s_2}\sin\beta_s + \tilde{t}_{r_2}\sin\beta_r)) && \text{(D-2)}\\ &= 2h_D - V_1[2t_{s_1}\sin\alpha_s + \rho^2(t_{s_2}\sin\alpha_s + t_{s_2}\sin\alpha_s)] && \text{(D-3)}\\ &= 2(h_D - V_1 t_{s_1}\sin\alpha_s(1+\rho^2) && \text{(D-4)}\\ &= 2h_D - h_D(1+\rho^2) = h_D(1-\rho^2) && \text{(D-5)} \end{aligned}$$

Similarly,

$$\begin{aligned} z_\xi &= V_1(t_{r_1} + \rho\tilde{t}_{s_2}\sqrt{1-\rho^2\sin^2\alpha_s} && \text{(D-6)}\\ &= V_1 t_{s_1}[\cos\alpha_s + \rho\sqrt{1-\rho^2\sin^2\alpha_s} && \text{(D-7)}\\ &= Z_{wb} + \frac{\rho V_1 t_m}{4}\sqrt{1-\rho^2\left(\frac{2h_D}{V_1 t_m}\right)^2} && \text{(D-8)}\\ &= Z_{wb} + \frac{\rho}{4}\sqrt{(V_1 t_m)^2 - \rho^2(2h_D)^2} && \text{(D-9)}\\ &= Z_{wb} + \frac{\rho}{4}\sqrt{4Z_{wb}^2 + 4h_D^2(1-\rho^2)} = Z_{wb} + \frac{\rho}{2}\sqrt{Z_{wb}^2 + h_D^2(1-\rho^2)} && \text{(D-10)} \end{aligned}$$

Finally,

$$\begin{aligned} m_\xi &= m_D + \frac{V_1}{2}(t_{s_1}\sin\alpha_s - t_{r_1}\sin\alpha_s) + \rho(\tilde{t}_{s_2}\sin\beta_s - \tilde{t}_{r_2}\sin\beta_r)) && \text{(D-11)}\\ &= m_D + \frac{V_1}{2}(t_{s_1}\sin\alpha_s - t_{s_1}\sin\alpha_s) + \rho^2(t_{s_2}\sin\alpha_s - t_{s_2}\sin\alpha_s) = m_D && \text{(D-12)} \end{aligned}$$

APPENDIX E

COMPUTATION OF TAKEOFF ANGLES FOR DIFFRACTED MULTIPLE

From Figure 14 we can immediately compute the takeoff angle of the diffracted receiver ray as

$$\alpha_r = \tan^{-1}\left[\frac{h_D + m_D - X_{diff}}{Z_{diff}}\right]. \qquad \text{(E-1)}$$

In this equation the depth of the diffractor is not known, but it can be calculated from the geometry of Figure E-1:

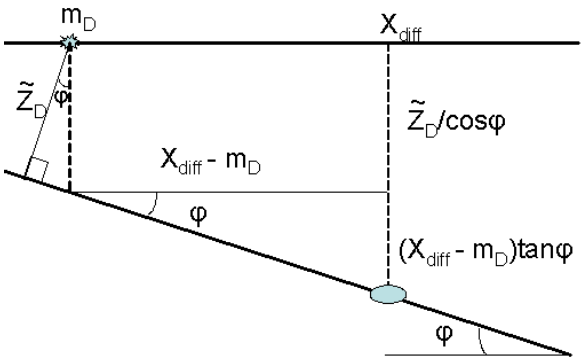

Figure E-1: Sketch showing the geometry of the zero surface half-offset diffracted multiple from a dipping water-bottom. gabriel1-mul_sktch13 [NR]

$$Z_{diff} = \frac{\tilde{Z}_D}{\cos\varphi} + (X_{diff} - m_D)\tan\varphi \qquad \text{(E-2)}$$

As we did for the diffracted multiple from the flat water-bottom, we can use the traveltime of the multiple at the zero surface-offset trace to compute $\tilde{Z}_D$, except that this time the computation is much more involved. Figure E-2 shows the basic geometry. From triangle ABC we have

$$[V_1(t_m(0)-t_{r_1}(0))]^2 = (2\tilde{Z}_D\cos\varphi + Z_{diff})^2 + (2\tilde{Z}_D\sin\varphi + (X_{diff}-m_D))^2, \qquad \text{(E-3)}$$

were t_{r_1} is the traveltime of the diffracted segment that, according to triangle DEF in Figure E-2 is given by

$$[V_1 t_{r_1}(0)]^2 = Z_{diff}^2 + (X_{diff}-m_D)^2. \qquad \text{(E-4)}$$

Replacing equations E-2 and E-4 into equation E-3 gives a quartic equation for $\tilde{Z}_D$ which can

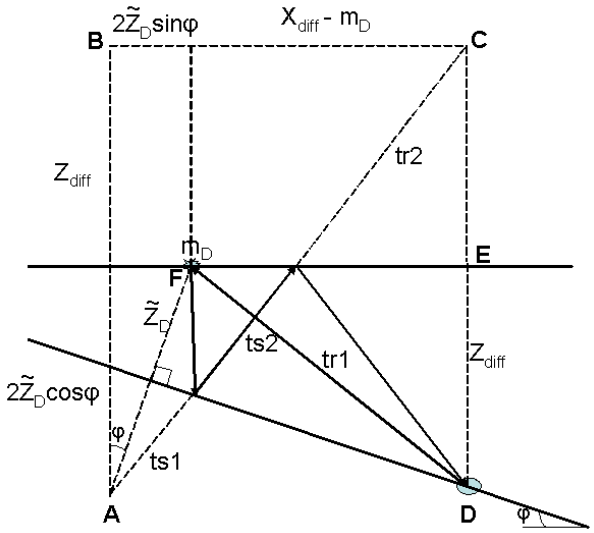

Figure E-2: Sketch to compute $\tilde{Z}_D$ in equations A-1, E-3 and E-4. gabriel1-mul_sktch14 [NR]

be solved numerically. Once $\tilde{Z}_D$ is known, we can easily compute Z_{diff} with equation E-2 and therefore α_r with equation E-1 in terms of the known quantities h_D, m_D, X_{diff} and $t_m(0)$. In order to compute α_s, we apply the law of sines to triangle ABC in Figure E-3 to get

$$\sin(\alpha_s + 2\varphi) = \frac{2\tilde{Z}_s\sin\varphi + (X_{diff}-m_D+h_D)}{V_1(t_m - t_{r_1})}, \qquad \text{(E-5)}$$

where $\tilde{Z}_s = \tilde{Z}_D - h_D\sin\varphi$ and $V_1 t_{r_1}$ is the length of the diffracted receiver ray and is given by

$$V_1 t_{r_1} = \sqrt{(h_D + m_D - X_{diff})^2 + Z_{diff}^2} \qquad \text{(E-6)}$$

Therefore, plugging equation E-6 into equation E-5 we get equation 50:

$$\alpha_s = \sin^{-1}\left[\frac{2\tilde{Z}_D\sin\varphi + (h_D + X_{diff} - m_D)}{V_1 t_m - \sqrt{(h_D + m_D - X_{diff})^2 + Z_{diff}^2}}\right] - 2\varphi. \qquad \text{(E-7)}$$

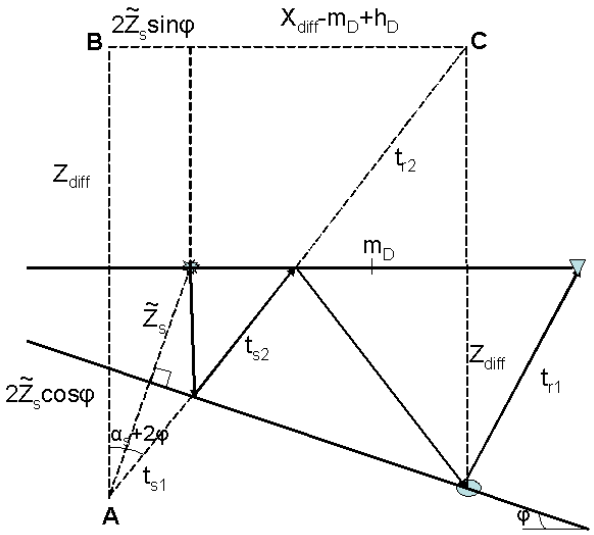

Figure E-3: Sketch to compute the takeoff angle of the source ray from a diffracted multiple. gabriel1-mul_sktch15 [NR]